# Modern Anti-Windup Design of Over-current Limiters for Grid-forming Inverters

Philippe Lefebvre
*Hydro-Québec's Research Institute (IREQ)*
*Hydro-Québec*
Varennes, Canada
https://orcid.org/0009-0000-5455-3020

Mathieu Lambert
*Hydro-Québec's Research Institute (IREQ)*
*Hydro-Québec*
Varennes, Canada
https://orcid.org/0000-0002-5562-4326

Dmitry Rimorov
*Hydro-Québec's Research Institute (IREQ)*
*Hydro-Québec*
Varennes, Canada
https://orcid.org/0000-0003-3068-5138

Innocent Kamwa
*Electrical and Computer Engineering*
*Université Laval*
Québec, Canada
https://orcid.org/0000-0002-3568-3716

***Abstract*—Grid-forming inverters must limit fault currents while preserving synchronism with the grid and their voltage-support behavior. However, current limiters interacting with integral action can trigger integrator windup and post-fault instability. In this paper, we addressed this by designing a dynamic anti-windup compensator for grid-forming inverters. We propose a way to represent the control so that it can be applied to the Direct Linear Anti-Windup architecture, which provides stability guarantees. Three-phase fault simulations showed that the proposed anti-windup prevents integrator accumulation during current saturation and avoids post-fault instability. The approach complements recent current-limiting strategies for grid-forming inverters by providing a constructive method for stability and performance guarantees with minimal changes to typical grid-forming inverter controls.**

***Index Terms*—Inverter-based resources, grid-forming inverter control, current limiting, anti-windup, linear matrix inequalities, stability**

## I. Introduction

Grid-forming (GFM) inverters are expected to replace existing inverter-based resources (IBR) for wind and solar energy, as the proportion of IBR with respect to synchronous generation increases. Unlike grid-following (GFL) inverters, which behave like a current source that are synchronized with the grid through the use of phase-locked loops, grid-forming inverters' behavior is similar to a voltage source behind an impedance. Recent reviews of state-of-the-art of GFM control strategies are given in [1], [2].

While it might seem logical and desirable only to have grid-forming inverters, because it is possible to emulate the behavior of a synchronous machine or perform better, it comes with several constraints. First, the DC bus must be strong and have sufficient energy stored to be able to maintain its voltage as constant as possible during a fault. Second, the power electronics are sensitive to over-currents (because they affect the junction temperature), which necessitate the use of current-limiting control strategies. A comprehensive review of current-limiting control strategies is detailed in [3]. Current limiting dominates the inverter's dynamics during and after a disturbance, and can strongly affect device-level and system-level stability (including synchronism). A source of undesirable post-fault instability is the integrator windup in the voltage control loop that causes the current limiter to clamp the current reference to the saturated value for an extended period of time after the fault has been cleared. Adding anti-windup helps by preventing integrator accumulation when the limiter is active.

The problem of limiting over-currents in GFM inverters remains a significant challenge. The two important questions are where in the overall control scheme the current limiter should be implemented and how to design a limiter/compensator to achieve fast current limitation without compromising post-fault recovery and stability. The solutions range from the virtual impedance method that belongs to the indirect methods of current limiting [4], [5], to the concept of virtual power and power reference and angle freeze that has been introduced to help improve the post-recovery transient stability [6]–[8]. Some methods embed the current limiter in the grid-forming architectures such as saturation-informed or cross-forming designs [9], [10]. Many require careful design and lack formal stability and performance guarantees or are difficult to implement in practice. By far one of the simplest and most practical solutions is to introduce a cascaded control structure with very fast internal current control loop, which belongs to the direct methods of current limiting [11]. Saturating the current control reference thus achieves the desired limiter performance but introduces the problem of integral windup. Therefore, designing an anti-windup compensation becomes critical to ensure fast regulator recovery and post-fault stability.

The paper addresses this challenge by applying a systematic design procedure to the anti-windup (AW) compensator design. Specifically, we use a Euclidean-norm saturation, embed it as a dead-zone input in the standard direct linear anti-

979-8-3315-8138-1

windup (DLAW) architecture, and synthesize a full-order AW compensator through the use of Algorithm 2 presented in [12].

The advantage of this method is the focus on maintaining some performance during the saturation as an explicit objective and the guarantee of global asymptotic stability (GAS) for a stable closed-loop linear plant. The results demonstrate that the designed AW compensator achieves the desired objective of fast recovery of post-fault conditions without jeopardizing large-signal stability.

This paper is organized as follows. The grid and control models are detailed in Sec. II. In Sec. III, we discuss the anti-windup algorithm. In Sec. IV, case studies are presented and the simulation results are shown. Finally, the conclusions of this paper are stated in Sec. V.

## II. Grid and control Model

### A. Grid and control

The grid for this study consists of an ideal voltage source with an RL line impedance. In order to be able to apply the DLAW algorithm, all grid quantities are expressed in the direct-quadrature ($dq$) frame and in per unit. The inverter is modeled as a controlled voltage source with an RL filter, as seen in Fig. 1.

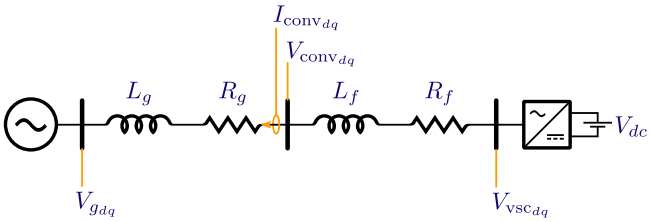


Figure 1. Grid model (part of the plant)

Since the grid quantities are expressed in the $dq$ frame, the nonlinear Park transformation from $abc$ to $dq$ is avoided. Furthermore, the grid quantities are in the inverter $dq$ frame instead of the grid $dq$ frame. It is applied upstream to the grid voltage $V_{g_{dq}}$ so that the whole system is linear time invariant. The inverter control used is a grid forming P-f, Q-V droop-controlled voltage source converter with the following droop control law:

$$\begin{aligned} \omega &= \omega_{\text{ref}} + m_p \left(P - P_{\text{ref}}\right), \\ V &= V_{\text{ref}} \ + n_q \left(Q - Q_{\text{ref}}\right). \end{aligned} \tag{1}$$

For the anti-windup design, the unconstrained controller needs to be linear time invariant. In order to achieve this, we kept the power calculation stage of the droop controller outside of the control and treated the deviations of the calculated powers from the setpoints $\Delta P = P - P_{\text{ref}}$ and $\Delta Q = Q - Q_{\text{ref}}$ as exogenous inputs to the controller as seen in Fig. 2.

The V-Q droop serves as the primary controller driving the voltage controller, and the current reference outputs of the voltage controller, $I_{d_{\text{ref}}}$ and $I_{q_{\text{ref}}}$, serves as the input to the saturation nonlinearity stage. The entire unconstrained controller is shown in figure 2.

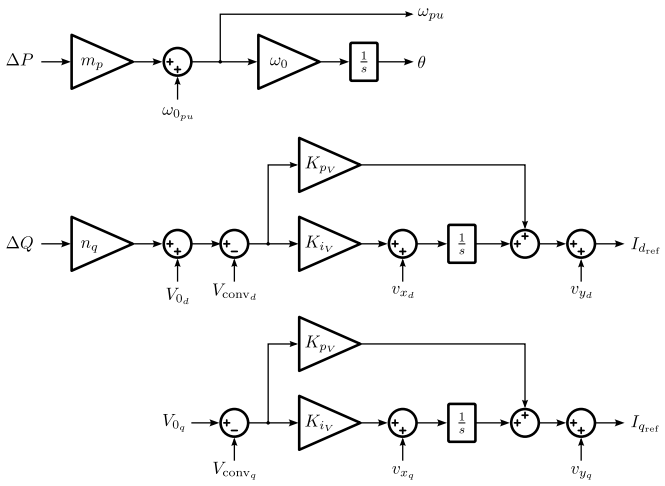


Figure 2. Unconstrained controller

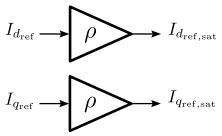


Figure 3. Saturation nonlinearity

### B. Euclidean-magnitude limiter and dead-zone

We impose a magnitude (Euclidean) current limit on the current references, i.e. $\|i_{dq,\text{ref}}\|_2 = \sqrt{i_{d,\text{ref}}^2 + i_{q,\text{ref}}^2}$. The nonlinear coefficient $\rho(i_{dq,\text{ref}})$ can be expressed as:

$$\rho(i_{dq,\text{ref}}) = \min\left(1, \ \frac{I_{max}}{\|i_{dq,\text{ref}}\|_2}\right) \tag{2}$$

We define $y_c = i_{dq,\text{ref}} \in \mathbb{R}^2$ and $u_0 = I_{\max} \in \mathbb{R}_{>0}$ and we can express the saturation function as $\text{sat}_{u_0}, (y_c) = \rho(y_c)\, y_c$ and the dead-zone input $\phi(y_c) = \text{sat}_{u_0}(y_c) - y_c$. The DLAW framework requires that the saturation nonlinearities via dead-zone signals satisfy a sector condition in order establish the stability guarantees and to derive the linear matrix inequalities (LMIs) [12]. Lemma 1 demonstrates that magnitude saturation fits the DLAW sector condition.

**Lemma 1** (Global sector condition for Euclidean-norm saturation)**.** Let $m \geq 1$, and $u_0 > 0$ be a scalar saturation limit. Let the Euclidean-norm (magnitude) saturation function be:

$$\text{sat}_{u_0}(y_c) = \rho(y_c)\, y_c, \qquad \rho(y_c) = \min\left(1, \ \frac{u_0}{\|y_c\|_2}\right), \tag{3}$$

for $y_c \in \mathbb{R}^m$, with the convention $\rho(0) = 1$. Let the associated dead-zone nonlinearity be:

$$\phi(y_c) = \text{sat}_{u_0}(y_c) - y_c. \tag{4}$$

Then, for any diagonal positive definite matrix $S \in \mathbb{R}^{m \times m}$, the following global sector inequality holds:

$$\phi(y_c)' S^{-1}\big(\phi(y_c) + y_c\big) \leq 0, \qquad \forall\, y_c \in \mathbb{R}^m. \tag{5}$$

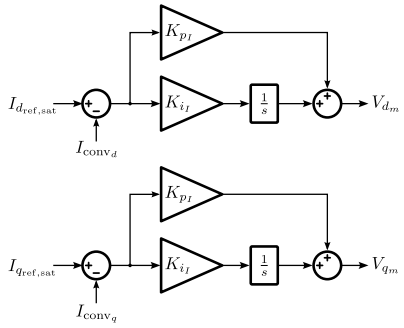


Figure 4. Current control loop (part of the plant)

*Proof.* We consider two cases.

*Case 1:* $\|y_c\|_2 \le u_0$. In this case $\rho(y_c) = 1$ in (3), so that $\mathrm{sat}_{u_0}(y_c) = y_c$ and hence $\phi(y_c) = 0$ from (4). Therefore

$$\phi(y_c)' S^{-1}\big(\phi(y_c) + y_c\big) = 0' S^{-1} y_c = 0 \le 0,$$

and (5) holds. The inequality also holds trivially for $y_c = 0$.

*Case 2:* $\|y_c\|_2 > u_0$. Define

$$\alpha = \frac{u_0}{\|y_c\|_2} \in (0,1).$$

Then by (3) we have $\mathrm{sat}_{u_0}(y_c) = \alpha y_c$, and from (4)

$$\phi(y_c) = \alpha y_c - y_c = (\alpha - 1) y_c, \qquad \phi(y_c) + y_c = \alpha y_c.$$

The sector inequality reduces to

$$\big(\alpha - 1\big) y_c' \, S^{-1}\big(\alpha y_c\big) = \big(\alpha - 1\big)\alpha \, y_c' \, S^{-1} y_c \le 0,$$

Because $\alpha \in (0,1)$, the product $\alpha(\alpha - 1)$ is strictly negative, and $y_c' \, S^{-1} y_c \ge 0$ since $S^{-1}$ is positive definite. Therefore

$$\phi(y_c)' S^{-1}\big(\phi(y_c) + y_c\big) = \big(\alpha - 1\big)\alpha \, y_c' \, S^{-1} y_c \le 0$$

for all $y_c$ with $\|y_c\|_2 > u_0$.

Combining the two cases, inequality (5) holds for all $y_c \in \mathbb{R}^m$. □

**Remark.** Lemma 1 and Remark 5 in [12] show that, for a component-wise saturation $\mathrm{sat}_{u_0}(\cdot)$, the associated dead-zone $\phi(y_c) = \mathrm{sat}_{u_0}(y_c) - y_c$ satisfies $\phi(y_c)' S^{-1}(\phi(y_c) + \omega) \le 0$ globally when $\omega = y_c$ is used in the modified sector condition. The lemma above shows that the same global sector inequality holds when the saturation is defined via the Euclidean norm as in (3). Therefore, the global DLAW synthesis conditions of Theorem 2 and Algorithm 2 in [12] remain valid when the component-wise saturation is replaced by a magnitude saturation.

## III. Problem Formulation and DLAW Architecture

We use the standard DLAW architecture from [12] and apply it to our system, where the plant and unconstrained controller are separated by the saturation nonlinearity, and where the anti-windup (AW) compensator is dynamic and full-order, i.e. $n_{aw} = n_p + n_c$. The dead-zone input entering the anti-windup compensator is given by $\phi(y_c) = \mathrm{sat}_{u_0}(y_c) - y_c$.

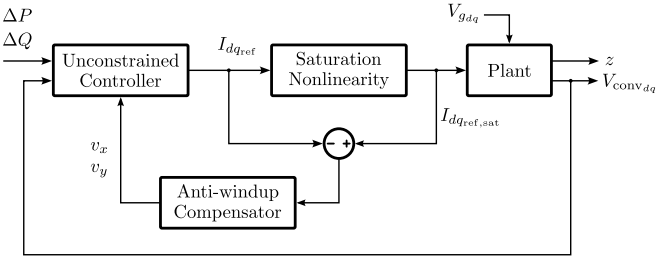


Figure 5. The DLAW architecture

The exogenous inputs $w$ are the deviations from the power setpoints and the grid voltage setpoints, i.e.:

$$w = [\Delta P,\ \Delta Q,\ \Delta v_{g,d},\ \Delta v_{g,q}] \tag{6}$$

where $\Delta P = P - P_{\text{ref}}$, $\Delta Q = Q - Q_{\text{ref}}$, $\Delta v_{g,d} = v_{g,d} - v_{g,d_{\text{ref}}}$, and $\Delta v_{g,q} = v_{g,q} - v_{g,q_{\text{ref}}}$.

Let the linear time invariant plant and linear time invariant unconstrained controller be represented together as:

$$\begin{aligned}
\dot{x}_p &= A_p x_p + B_{pu}\,\mathrm{sat}_{u_0}(y_c) + B_{pw}\,w \\
y_p &= C_p x_p + D_{pu}\,\mathrm{sat}_{u_0}(y_c) + D_{pw}\,w \\
z &= C_z x_p + D_{zu}\,\mathrm{sat}_{u_0}(y_c) + D_{zw}\,w \\
\dot{x}_c &= A_c x_c + B_c y_p + B_{cw}\,w \\
y_c &= C_c x_c + D_c y_p + D_{cw}\,w
\end{aligned} \tag{7}$$

with $\mathbf{\Delta} = I_m - D_c D_{pu}$ nonsingular. The unsaturated closed-loop matrix is:

$$\mathbb{A} = \begin{bmatrix} A_p + B_{pu}\mathbf{\Delta}^{-1} D_c C_p & B_{pu}\mathbf{\Delta}^{-1} C_c \\ B_c\left(I_p + D_{pu}\mathbf{\Delta}^{-1} D_c\right) C_p & A_c + B_c D_{pu}\mathbf{\Delta}^{-1} C_c \end{bmatrix} \tag{8}$$

and is required to be Hurwitz (nominal stability).

### A. Anti-windup architecture

We use the standard DLAW form with full-order dynamic AW:

$$\begin{aligned}
\dot{x}_p &= A_p x_p + B_{pu}\,\mathrm{sat}_{u_0}(y_c) + B_{pw}\,w \\
y_p &= C_p x_p + D_{pu}\,\mathrm{sat}_{u_0}(y_c) + D_{pw}\,w \\
z &= C_z x_p + D_{zu}\,\mathrm{sat}_{u_0}(y_c) + D_{zw}\,w \\
\dot{x}_c &= A_c x_c + B_c y_p + B_{cw}\,w + v_x \\
y_c &= C_c x_c + D_c y_p + D_{cw}\,w + v_y \\
\dot{x}_{aw} &= A_{aw} x_{aw} + B_{aw}(\mathrm{sat}_{u_0}(y_c) - y_c) \\
v_x &= \begin{bmatrix} I_{n_c} & 0 \end{bmatrix}(C_{aw} x_{aw} + D_{aw}(\mathrm{sat}_{u_0}(y_c) - y_c)) \\
v_y &= \begin{bmatrix} 0 & I_m \end{bmatrix}(C_{aw} x_{aw} + D_{aw}(\mathrm{sat}_{u_0}(y_c) - y_c))
\end{aligned} \tag{9}$$

where $v_x$ and $v_y$ are the anti-windup output signals. We chose the performance signals $z$ to represent, in this work, the discrepancy between the saturated reference current and the measured current, which are given by:

$$z = W_P \begin{bmatrix} I_{d_{\text{ref,sat}}} - I_{\text{conv}_d} \\ I_{q_{\text{ref,sat}}} - I_{\text{conv}_q} \end{bmatrix} \tag{10}$$

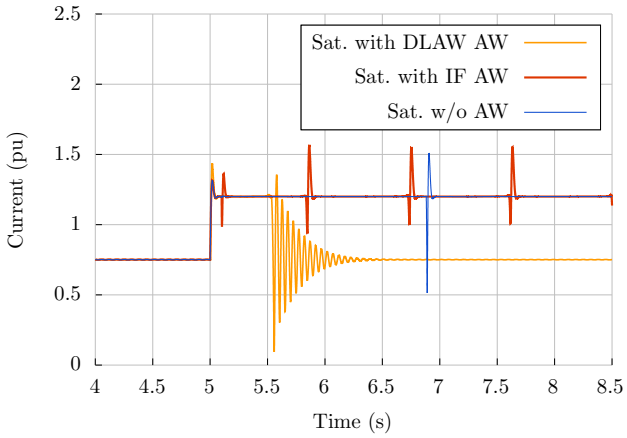


Figure 6. Current magnitude limited to 1.2 pu during a 100 ms three-phase fault with a grid with a short-circuit ratio of 15 for the saturated current a) with the DLAW AW b) with the IF AW and c) without AW.

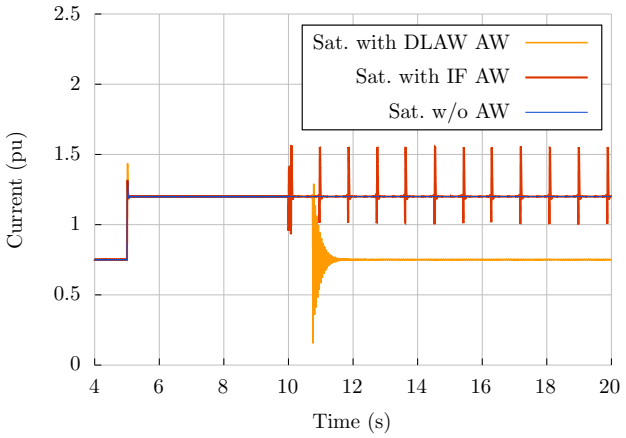


Figure 8. Current magnitude limited to 1.2 pu during a 5 seconds three-phase fault with a grid with a short-circuit ratio of 15 for the saturated current a) with the DLAW AW b) with the IF AW and c) without AW.

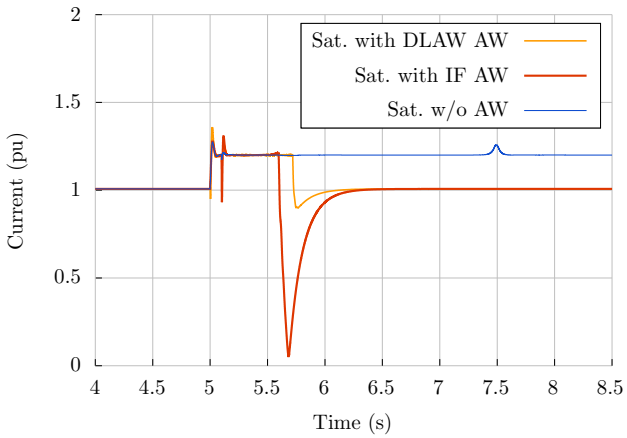


Figure 7. Current magnitude limited to 1.2 pu during a 100 ms three-phase fault with a grid with a short-circuit ratio of 1.5 for the saturated current a) with the DLAW AW b) with the IF AW and c) without AW.

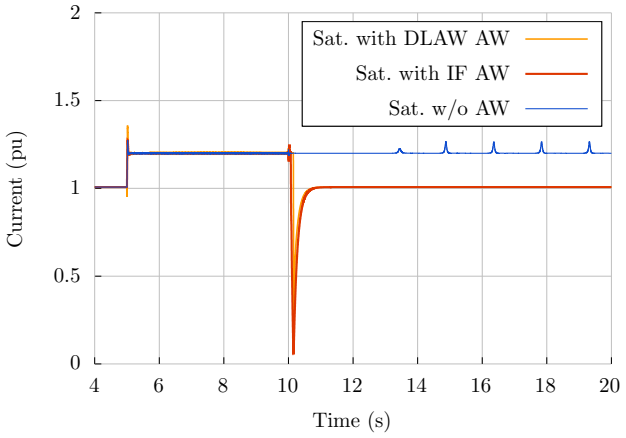


Figure 9. Current magnitude limited to 1.2 pu during a 5 seconds three-phase fault with a grid with a short-circuit ratio of 1.5 for the saturated current a) with the DLAW AW b) with the IF AW and c) without AW.

Where $W_P$ is a specific weight for performance, set to 5 in this work.

After defining $z$, we can define $C_z$, $D_{zu}$ and $D_{zw}$. In our case these matrices are:

$$C_z = W_P \begin{bmatrix} 0 & 0 & -I_{\text{conv}_d} & 0 \\ 0 & 0 & 0 & I_{\text{conv}_q} \end{bmatrix}$$

$$D_{zu} = W_P \begin{bmatrix} I_{d_{\text{ref,sat}}} & 0 \\ 0 & I_{q_{\text{ref,sat}}} \end{bmatrix} \tag{11}$$

$$D_{zw} = \mathbf{0}_{2\times 4}$$

### B. LMI Synthesis

We follow the standard three-stage procedure from Algorithm 2 in [12], which are: dilated LMIs, congruence to recover $Q$, and convex AW synthesis where $Q$ is fixed.

If $A_p$ is Hurwitz and (19) in [12] is feasible, the saturated closed loop with the designed AW exhibits: (i) small-signal preservation (when $\phi = 0$); (ii) GAS for $w \equiv 0$; and (iii) an induced $L_2$ bound $\|z\|_2 \leq \gamma \|w\|_2$.[1] This procedure yields global asymptotic stability for $w \equiv 0$ and the above $L_2$ bound [12].

## IV. Case Studies and Results

In this section, simulation studies are conducted to characterize the performance of the DLAW anti-windup approach. For a three-phase fault scenario, we compare the system response with no anti-windup, with a baseline integral-freeze (IF) anti-windup, and with the proposed DLAW anti-windup method presented in this work. The integral freeze AW replaces the input of the integrator of the voltage PI control with a signal value of zero when the current saturation is reached.

The first case study is a three-phase fault starting at the fifth second and lasting 100 ms on a strong grid with a short circuit

[1]Regional variants and fixed-order options follow the same pattern with generalized-sector LMIs, which are omitted for brevity. For additional details, see [12].

ratio (SCR) of 15, where the results are shown in Fig. 6. The results for a weak grid with a SCR of 1.5 are presented in Fig. 7.

As it can be seen in the results of Fig. 6 for the strong grid case, without AW, the limiter clamps the current and the controller integrator winds up, producing a sluggish and potentially unstable post-fault recovery. The same problem occurs with the integral feeze AW where the limiter clamps the current and the current signal is trapped in a similar limit cycle as in the case without AW. With the synthesized DLAW control, the dead-zone signal drives $v_x$ and $v_y$ to cancel the windup. The current limiting is respected, and the states converge to the nominal equilibrium once exogenous input disturbance subsides, i.e. $\begin{bmatrix}\Delta v_{g,d}\\ \Delta v_{g,q}\end{bmatrix} \to 0$.

The results in Fig. 6 show the weak grid case with the inverter current magnitude having the same behavior without AW. The IF AW manages to work under a weak grid. The DLAW AW also work similarly to the IF AW but with a smaller current incursion.

The second case study compares a strong grid Fig. 8 and a weak grid Fig. 9 for a three-phase 5 seconds fault starting at the fifth second. The 5 seconds three-phase fault is a test where we neglect the effects of the protection to stress the cumulative effect of integration and see whether the anti-windup can recover the unconstrained response even after very long integral windups. Fig. 8 and Fig. 9 show the saturated current magnitude with: a) the current saturated inverter without AW, b) the current saturated inverter with integral freeze AW and c) the current saturated inverter with DLAW AW.

The results of Fig. 8 in a strong grid show that DLAW anti-windup is able to recover after the fault even with an extended integral wind-up period. In the weak grid case shown in Fig. 9, we see that the IF AW and DLAW AW have similar performance.

## V. Conclusion

In this paper it was shown that using the DLAW anti-windup method for the over-current limiting can mitigate instability problems on a droop-controlled inverter.

We presented a constructive method for anti-windup design for GFM inverters with magnitude current limiting, using the DLAW architecture and LMI-based Algorithm 2 of [12]. We have adapted the model so that it satisfies the requirements for the algorithm and have shown the applicability of the Euclidean magnitude saturation. The method preserves nominal small-signal behavior, prevents integral windup during current saturation, and guarantees global asymptotic stability with an $L_2$ bound. Simulations on a droop-controlled 1-MW inverter confirmed robust post-fault recovery while enforcing current limits.

Furthermore, the GAS result of Algorithm 2 holds under the standard intrinsic limitations: global exponential stability with bounded input is impossible unless the plant is exponentially stable; with a Hurwitz $A_p$, DLAW achieves GAS with an $L_2$ bound. For marginally stable or exponentially unstable plants, regional designs (generalized sector) or nonlinear MRAW are appropriate alternatives (outside the scope of this paper).

In the future, extension to this work will involve the case of single-phase current limiting, as most contingencies involve single line to ground faults [3]. The behavior of this current limiter in the case of Type-IV wind turbine connected to the DC bus machine-side inverter will also be the topic of future work.


## Acknowledgment

The Authors would like to thank their colleague Dr. Hind Chit Dirani for the careful reviewing of this paper.


## References


[1] M. Tozak, S. Taskin, I. Sengor, and B. P. Hayes, "Modeling and control of grid forming converters: A systematic review," *IEEE Access*, vol. 12, pp. 107 818–107 843, 2024.

[2] N. Mohammed, H. Udawatte, W. Zhou, D. J. Hill, and B. Bahrani, "Grid-forming inverters: A comparative study of different control strategies in frequency and time domains," *IEEE Open J. Ind. Electron.*, vol. 5, pp. 185–214, 2024.

[3] N. Baeckeland, D. Chatterjee, M. Lu, B. Johnson, and G.-S. Seo, "Overcurrent limiting in grid-forming inverters: A comprehensive review and discussion," *IEEE Trans. Power Electron.*, vol. 39, no. 11, pp. 14 493–14 517, Nov 2024.

[4] A. D. Paquette and D. M. Divan, "Virtual impedance current limiting for inverters in microgrids with synchronous generators," *IEEE Trans. Ind. Appl.*, vol. 51, no. 2, pp. 1630–1638, 2015.

[5] G. Denis, T. Prevost, M.-S. Debry, F. Xavier, X. Guillaud, and A. Menze, "The Migrate project: the challenges of operating a transmission grid with only inverter-based generation. A grid-forming control improvement with transient current-limiting control," *IET Renew. Power Gener.*, vol. 12, no. 5, pp. 523–529, 2018.

[6] K. V. Kkuni and G. Yang, "Effects of current limit for grid forming converters on transient stability: Analysis and solution," *Int. J. Electr. Power Energy Syst.*, vol. 158, p. 109919, 2024.

[7] Y. Laba, A. Bruyère, F. Colas, and X. Guillaud, "Virtual power-based technique for enhancing the large voltage disturbance stability of HV grid-forming converters," in *EPE ECCE Europe*, 2023, pp. 1–8.

[8] S. Jiang, Y. Zhu, T. Xu, and G. Konstantinou, "Current-synchronization control of grid-forming converters for fault current limiting and enhanced synchronization stability," *IEEE Trans. Power Electron*, vol. 39, no. 5, pp. 5271–5285, May 2024.

[9] M. A. Desai, X. He, L. Huang, and F. Dörfler, "Saturation-informed current-limiting control for grid-forming converters," *Electr. Power Syst. Res.*, vol. 234, p. 110746, 2024.

[10] X. He, M. A. Desai, L. Huang, and F. Dörfler, "Cross-forming control and fault current limiting for grid-forming inverters," *IEEE Trans. Power Electron.*, vol. 40, no. 3, pp. 3980–4007, 2025.

[11] N. Baeckeland and G.-S. Seo, "Large-signal stability improvement of parallel grid-forming inverter-driven black start," in *IEEE PES ISGT Conference*, Washington, DC, USA, Feb 2024, pp. 1–5.

[12] S. Galeani, S. Tarbouriech, M. Turner, and L. Zaccarian, "A tutorial on modern anti-windup design," *Eur. J. Control*, vol. 15, no. 3-4, pp. 418–440, 2009.